ADVANCED MATERIALS
www.advmat.de

Visually Imperceptible Liquid-Metal Circuits for Transparent, Stretchable Electronics with Direct Laser Writing

*Chengfeng Pan, Kitty Kumar, Jianzhao Li, Eric J. Markvicka, Peter R. Herman, and Carmel Majidi**

A material architecture and laser-based microfabrication technique is introduced to produce electrically conductive films (sheet resistance = 2.95 Ω sq^{-1}; resistivity = 1.77 × 10^{-6} Ω m) that are soft, elastic (strain limit >100%), and optically transparent. The films are composed of a grid-like array of visually imperceptible liquid-metal (LM) lines on a clear elastomer. Unlike previous efforts in transparent LM circuitry, the current approach enables fully imperceptible electronics that have not only high optical transmittance (>85% at 550 nm) but are also invisible under typical lighting conditions and reading distances. This unique combination of properties is enabled with a laser writing technique that results in LM grid patterns with a line width and pitch as small as 4.5 and 100 µm, respectively—yielding grid-like wiring that has adequate conductivity for digital functionality but is also well below the threshold for visual perception. The electrical, mechanical, electromechanical, and optomechanical properties of the films are characterized and it is found that high conductivity and transparency are preserved at tensile strains of ≈100%. To demonstrate their effectiveness for emerging applications in transparent displays and sensing electronics, the material architecture is incorporated into a couple of illustrative use cases related to chemical hazard warning.

C. F. Pan, Dr. K. Kumar
Integrated Soft Materials Lab
Mechanical Engineering
Carnegie Mellon University
Pittsburgh, PA 15213, USA
Dr. J. Z. Li, Prof. P. R. Herman
Electrical and Computer Engineering
University of Toronto
Toronto, ON M5S 3G4, Canada
E. J. Markvicka
Integrated Soft Materials Lab
Robotics Institute
Carnegie Mellon University
Pittsburgh, PA 15213, USA
Prof. C. Majidi
Integrated Soft Materials Lab
Mechanical Engineering
Material Science and Engineering
Robotics Institute
Carnegie Mellon University
Pittsburgh, PA 15213, USA
E-mail: cmajidi@andrew.cmu.edu
The ORCID identification number(s) for the author(s) of this article can be found under https://doi.org/10.1002/adma.201706937.

DOI: 10.1002/adma.201706937

Transparent conductors like indium tin oxide (ITO), gallium-doped zinc oxide (GZO),[1] and poly(3,4-ethylenedioxythiophene)-poly(styrenesulfonate) (PEDOT:PSS) have played a central role in the development of touch-display computing,[2–4] wearable devices,[5,6] photovoltaics,[7,8] and other flexible and optoelectronic thin-film technologies that require robust electronic interfaces with high optical transmittance. However, the successful integration of these devices into future "soft-matter" technologies for wearable computing,[9,10] human–machine interfaces,[11,12] bionic contacts,[13] or direct interfacing of living neurons with resistive switching devices,[14] demands a new generation of "optically-clear" conductors that are primarily engineered from materials that match the mechanical properties of soft biological tissues. Efforts in this domain have been largely focused on two discrete domains: synthetic composite materials (e.g., elastomers with conductive nanoparticle filler) and deterministic multi-material architectures (patterned metal films on an elastomer substrate) formed by combining high-performance conducting materials with stretchable polymers.

The first class includes a variety of stretchable conductive materials that have been developed by loading clear elastic polymers and gels with visually imperceptible particulates such as carbon nanotubes and graphene,[15–18] metal nanowires,[19,20] or metal salt.[10] While these composite materials show promising stretchability (elastic strain limit, ε_{max} > 100%), low sheet resistance (R_s < 10 Ω sq^{-1}), and optical transparency (T ≈ 70–98%), they exhibit significant electromechanical and optomechanical coupling and/or hysteresis.[21,22] The second class of "deterministic" transparent conductors have been demonstrated with lithographically patterned meshes of gold or copper on a soft polymer substrate.[23–25] The balance between R_s and T is achieved by tailoring the thickness of the conductive material and the spatial distance between visually perceptible opaque features. These multimaterial architectures, however, show poor stretchability (ε_{max} ≈ 10–50%) and fail mechanically due to out-of-plane deformation of the intrinsically inextensible metal mesh.

In recent years, patterned arrays of Ga-based liquid-metal (LM) alloy (eutectic gallium indium; EGaIn) on elastomeric substrates

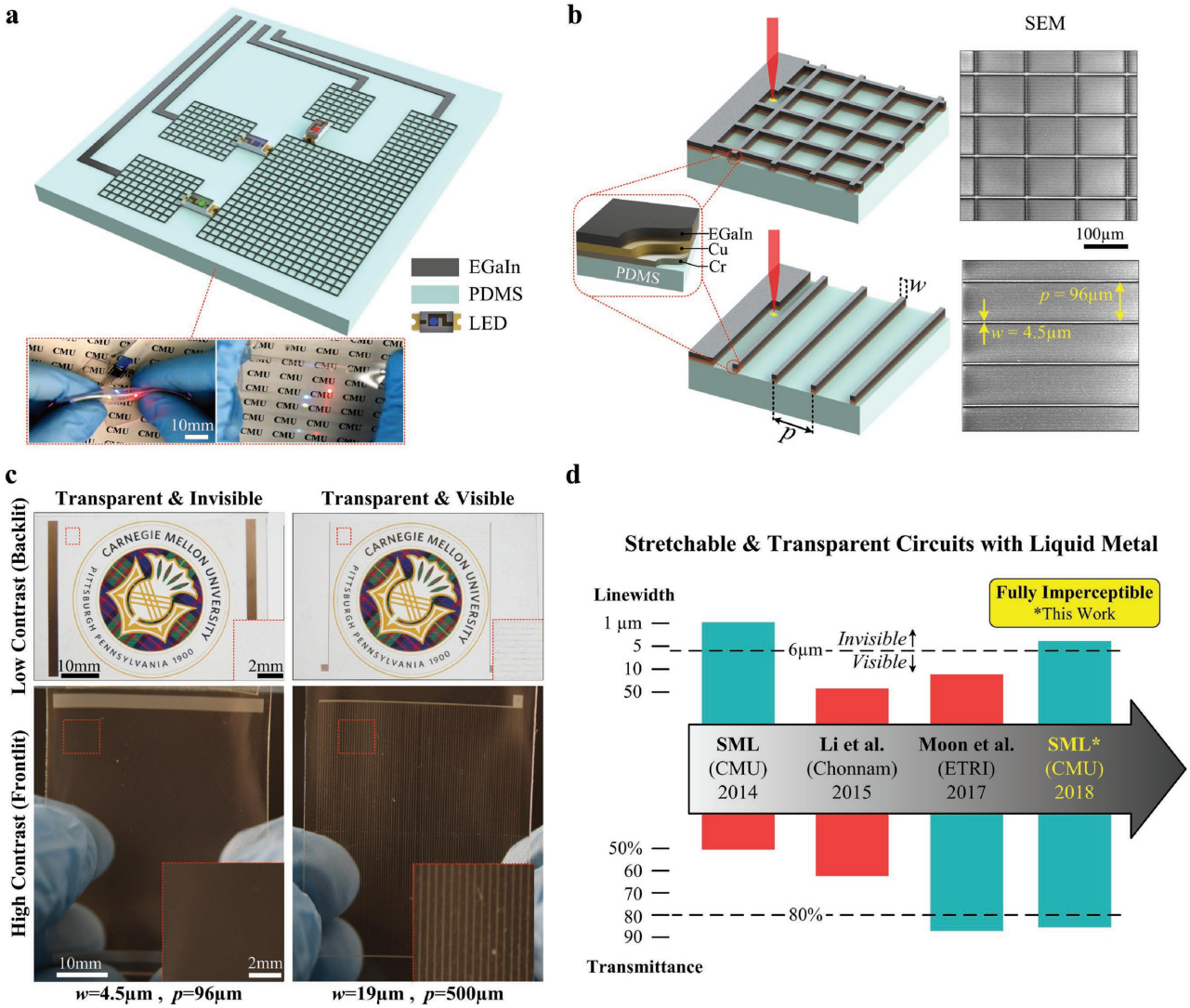

Figure 1. a) Schematic of optically clear electronics comprised of grid-like LM circuitry and integrated microelectronic components; (inset) representative circuit showing an exceptional combination of mechanical deformability, electrical functionality, and optical transparency. b) The schematic and SEM images of the square grid and parallel line patterns of 4.5 μm wide EGaIn traces; the LM patterns are patterned by microscale laser ablation of the thin-film architecture (LM/Copper/Chromium) on a PDMS substrate. c) Photographs of parallel line pattern with line widths (w)/pitches (p) of 4.5 μm/96 μm (left) and 20 μm/500 μm (right) under backlit (low contrast) and frontlit (high contrast) conditions; the grated pattern of 20 μm wide LM traces is resolved in both high and low contrast conditions, whereas the pattern of 4.5 μm wide traces is visually imperceptible. d) Progress in optically clear and stretchable LM circuits showing past[30,33,36] and current achievements in improving optical transmittance and reducing trace linewidth and pitch to below the threshold for visibility under general reading distances and lighting conditions.

have been explored as an alternative to solid-state metals for highly stretchable circuit wiring,[26–28] and liquid-phase robotics.[29] Lithographically patterned grids of 20 μm wide LM traces on a PEDOT:PSS substrate have been shown to exhibit a strain limit of $\varepsilon_{max} \approx 40\%$ and sheet resistance of $R_s = 2.3\ \Omega\ sq^{-1}$.[30] These grids yield a high transmittance of $T \approx 88\%$ due to the large trace pitch (i.e., low LM filling fraction), which results in large openings for light to pass through. While invisible at close distance (e.g., on a contact lens), grids with these trace dimensions can be seen when placed at a natural reading distance.[31] This is because 20 μm wide opaque traces with a 400 μm pitch (i.e., larger than the grating acuity threshold of 75–100 μm[32]) on a transparent substrate will have sufficient contrast to be visually resolved by the eye (see Section S1 in the Supporting Information for details). Therefore, such circuits are unsuitable for applications in touch screens and electronic displays that require high optical clarity over a complete focal range. LM patterns with pitch (≈2 μm) below the grating acuity threshold of human eyes have been demonstrated in the past with stamp lithography.[33] However, the high trace density resulted in a low transmittance and the patterning method has not been shown to be compatible with large-area circuit fabrication. The facile fabrication of optically clear, large-area, highly transparent LM circuitry with feature size below the threshold of visual perception remains a grand challenge within the field.[34,35]

Here, we present a materials architecture and rapid microfabrication approach for creating optically clear LM circuits (**Figure 1**a) that exhibit an exceptional combination

of low resistivity ($\rho = 1.77 \times 10^{-6}$ Ω m) and sheet resistance ($R_s = 2.95$ Ω sq^{-1}), high strain limit ($\varepsilon_{max} > 100\%$), high transparency (up to $T = 85.3\%$ at 550 nm), and low trace width ($w \geq 4.5$ µm). The circuits are directly patterned on a transparent poly(dimethylsiloxane) (PDMS; Sylgard 184, Dow Corning) elastomer substrate with ablative laser micromachining. To help adhere the EGaIn and PDMS, a "bi-phasic" architecture was adopted in which a thin metal film—in this case sputter deposited Cr/Cu—was coated on the PDMS prior to EGaIn deposition and patterning.[36–38] Referring to Figure 1b, picosecond laser ablation was optimized for clean subtractive processing of metal films into conductive grid lines as narrow as 4.5 µm placed at a pitch of less than 100 µm, which presented a visually imperceptible pattern with high transparency for typical reading distances and lighting conditions. The fabricated LM wiring can be readily interfaced with conventional circuit components (e.g., lead wiring, packaged microelectronics, or light emitting diode (LED) chips) to enable optically clear digital electronics. As with ITO and other transparent conductors used in personal electronics, the circuits were not visible when placed: (i) over text, (ii) in low contrast and backlit conditions, and (iii) high contrast and frontlit conditions (Figure 1c). Compared with previous efforts in LM patterning, the CAD/CAM-compatible laser direct writing method presented here enables rapid prototyping of optically transparent circuits with LM traces that are visually imperceptible for any prescribed focal distance. While previous work has demonstrated either invisible traces (i.e., linewidth < 6 µm & pitch < 100 µm)[33] or a high optical transmittance ($T \geq 80\%$),[30] the grid-like circuits presented here are the first to demonstrate both (Figure 1d).

LM grids were fabricated with a variety of trace widths in order to address the following: (i) validate an optimal fabrication method by comparing electrical, mechanical, and electromechanical properties of 20 µm wide LM traces with measurements from previous studies,[30] (ii) confirm that optical transmittance is governed by fraction of the substrate area covered by LM and is virtually independent of the trace width, and (iii) establish that the influence of trace width on optical clarity of LM conductor depends in the context of various visual conditions (e.g., focal distance, contrast, lighting).

We begin by showing that LM conductors fabricated with ablative laser processing exhibit a sheet resistance, strain limit, and electromechanical response that is consistent with LM conductors created with existing patterning methods. Parallel line arrays of 20 µm wide LM traces with 500 µm pitch (LM filling fraction, $\phi = 3.8\%$) were patterned over a 7×7 mm^2 area on PDMS substrates by scanning a Nd:YAG laser (ProtoLaser U3; LPKF Laser & Electronics AG; see Experimental Section for details) of 355 nm wavelength to selectively remove the metal film while minimizing substrate damage. The use of a 355 nm Nd:YAG laser to pattern EGaIn on a soft elastomer substrate for the purposes of non-transparent hybrid LM-microchip electronics had previously been reported by the senior author.[39] Here, the objective is to compare the characterization results of laser-processed LM patterned conductors with LM conductors comprised of 20 µm wide traces defined by nonablative techniques (e.g., photolithography[30]). The measured initial sheet resistance ($R_s = 1.7$ Ω sq^{-1}) of the laser processed LM parallel line grid is smaller than the 2.3 Ω sq^{-1} value[26] measured in the lithographically-defined square grids. This is in spite of having 2.5 × less area filling fraction—i.e. $\phi = 4\%$ (straight-line grid pitch = 500 µm) for the laser-patterned sample versus $\phi = 10\%$ (square grid pitch = 400 µm) for the sample in ref. [26]. Together, this suggests that the thermal ablative laser process does not degrade the electrical properties of the EGaIn alloy (for example, due to overablation, excessive gallium oxidation, etc.) and has potential as a reliable method for LM grid patterning.

A typical evolution of the relative change in resistance ($\Delta R/R_0$) of the fabricated LM conductor as a function of strain applied along the trace length (longitudinal strain, ε_x) and width (transverse strain, ε_y) is presented in **Figure 2**a,b, respectively. In the first cycle, the sample was first stretched by 50%, which is well below the strain limit of pristine PDMS substrate, $\varepsilon_{PDMS} \approx 165\%$ (see Figure S3 in Section S2, Supporting Information for mechanical stress–strain data) and then relaxed to its original length. In each consecutive cycle, the strain is increased until a mechanical failure is observed. The optical images of laser patterned biphasic metallic grid (LM–Cu–Cr) and Cu–Cr thin film at different elongation strains in longitudinal and transverse direction, and when cycled back to the relaxed state in both cases are presented in Figure S4 in Section S3 (Supporting Information). In the case of longitudinal elongation (Figure 2a), the relative change in resistance increases linearly with the applied strain (slope ≈ 1). After all three incremental strain cycles, the resistance returned to the initial value ($R_0 = 1.7$ Ω) upon relaxing. It should be noted that R_0 shares the same magnitude as sheet resistance (R_s) since $R_s = R_0 \times \{\text{width}\}/\{\text{length}\}$ and the sample has square dimensions. The sample mechanically failed at $\varepsilon_x = 165\%$ strain, which is within the range of strain limit values measured for pristine PDMS (see Figure S3 in Section S2, Supporting Information). Furthermore, the electromechanical response of the fabricated samples was similar to the previous work,[30] where a ≈55% change in resistance had been reported at a 60% elongation strain. Interestingly, resistance was observed to decrease when the sample was stretched in the transverse direction (Figure 2b). We attribute this to the incompressibility of the elastomer and a "Poisson's effect" that results in a decrease in trace length during transverse stretch. However, transverse stretch also results in significant hysteresis, which is most pronounced for strains ≥75% and is likely related to the permanent wrinkling of the underlying Cu–Cr thin film at these high strains (evident in the $\varepsilon_y' = 0\%$ panel of Cu–Cr thin film in Figure S4 in Section S3, Supporting Information). Under transverse stretching, the sample failed mechanically at a strain value of $\varepsilon_y = 140\%$. Overall, the results in Figure 2a,b provide further evidence that laser ablation is a reliable patterning method that does not significantly alter the intrinsic properties of the PDMS or EGaIn.

As shown in Figure 2c, the LM conductor demonstrates largely consistent behavior when cyclically strained between $\varepsilon = 0\%$ and 50% over multiple loading cycles. As in Figure 2a, there is no evidence of significant electromechanical hysteresis for samples loaded in the longitudinal direction while such hysteresis is evident for transverse loading. However, this transverse hysteresis is associated with a small decrease in resistance (3%) after the first loading cycle, which we believe arises from the permanent wrinkling of the underlying Cu–Cr adhesive thin film. For subsequent loading cycles, the electromechanical response remains stable—shown in Figure 2d for 3000 cycles.

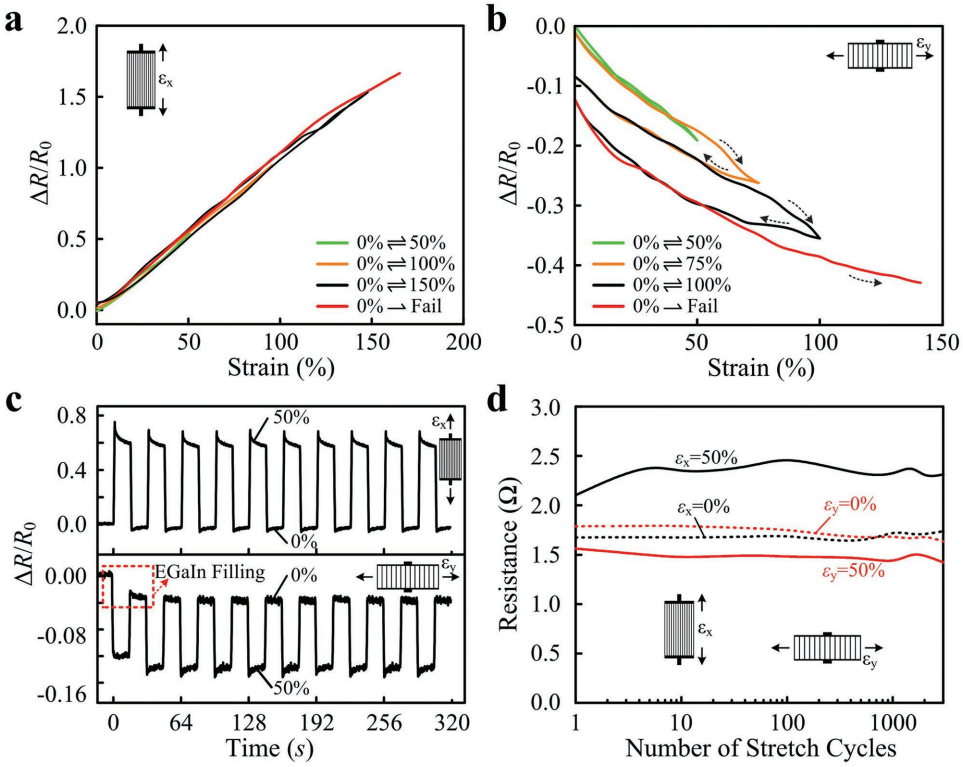

Figure 2. Electromechanical response of laser patterned LM conductor as a function of strain applied in the direction parallel to the trace a) length (ε_x, strain applied in longitudinal direction) and b) width (ε_y, transverse strain). In both a,b), the maximum applied strain increases in each consecutive cycle until failure. c) Electromechanical response of the sample when cyclically strained to maximum strain of 50% over ten cycles in longitudinal (top) and transverse (bottom) direction. d) Resistance of the conductor at 50% elongation in longitudinal (black) and transverse (red) direction and in-between relaxed states over 3000 cycles.

The results of the cyclical study suggest that the laser writing process provides a mechanically robust circuit without unduly influencing the intrinsic mechanical, electrical, or electromechanical properties of the EGaIn–PDMS architecture.

Having established the consistency in material performance (sheet resistance, strain limit, electromechanical coupling) between direct laser ablation and other LM-patterning techniques, we next set out to engineer visually imperceptible LM circuitry with reduced trace width. For the length-scales of interest, film transmittance (T) was evaluated by ignoring diffraction effects and simply following the area filling fraction (ϕ) of the opaque LM according to the relationship $T = (1 - \phi)$ T_{PDMS} Here, T_{PDMS} is the transmittance of the bare PDMS and ϕ was estimated from the LM wire width, w, and grating period (pitch) p, e.g. $\phi = w/p$ for the case of parallel lines. The value for T_{PDMS} was obtained by measuring the optical transmittance through a PDMS substrate in which the biphasic metal coating (i.e., EGaIn–Cu–Cr) is fully removed with the same laser parameters used for line patterning. Calculated in this way, the transmittance through the grated LM structure improved asymptotically toward 89% with increasing ϕ relative to the bare PDMS transmittance.

In addition to demonstrating high transmittance, the opaque LM wire pattern must not be resolvable by the unaided eye under lighting conditions that are typical for the prescribed applications. This was addressed by narrowing the LM wire width with a higher resolution laser ablation process, centered on a short-pulsed laser (Lumera, Hyper Rapid 50; pulse duration = 12 ps)[40] and high-resolution motion stages. LM patterns were generated with LM line widths (w) as small as 4.5 µm and the grating period (p) in a range of 17.5 to 96 µm, which correspond to LM filling fractions of $\phi = 26.6\%$ to 4.5%, respectively (see Table S1 in Section S4, Supporting Information for grating parameters). Figure 1c shows optical images of two samples with w = 4.5 µm and p = 96 µm (left) and w = 19 µm and p = 500 µm (right), where the wire grid pattern is visually imperceptible only for the 4.5 µm wire width under both high and low contrast conditions.

To validate our theoretical model for transmittance, we also fabricated a second set of parallel line arrays of 50 µm wide LM wires with periodicity ranging from 125 to 500 µm, which correspond to ϕ = 42% to 10%, respectively. The reference transmittance of the bare PDMS substrate, following full laser removal of metal coating, yielded $T_{PDMS} \approx 89\%$, determined for an 18 cm × 15 cm area ablated by the Lumera and LPKF lasers. The surface topography maps of the laser-exposed PDMS surface are obtained with atomic force microscopy (AFM) and presented in Figure S6 in Section S4 (Supporting Information). In these reference samples, the laser processes optimized for 4.5 and 50 µm straight-line gratings were applied by the Lumera and LPKF lasers, respectively, and further details on the T_{PDMS} measurement and PDMS surface quality are presented in Section S4 (Supporting Information). **Figure 3**a shows the optical transmittance measured through the grated patterns of 4.5 µm

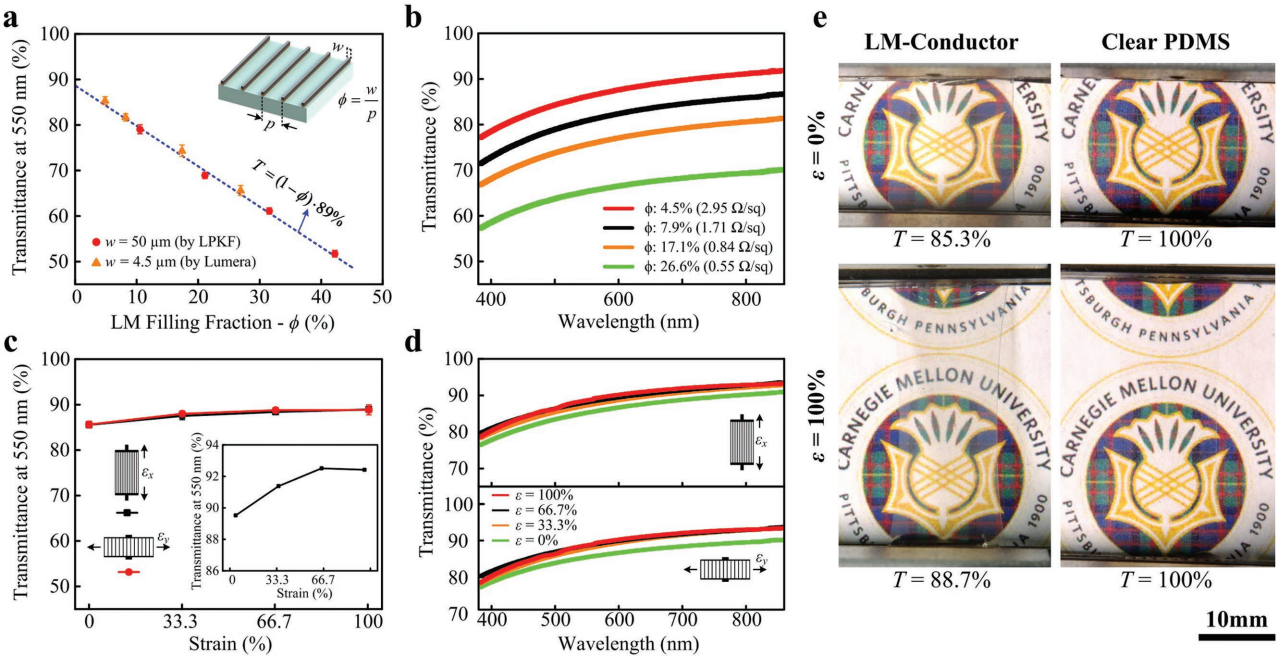

Figure 3. a) Transmittance at 550 nm wavelength through LM grating patterns of 4.5 and 50 μm wide traces as a function of EGaIn filling fraction (ϕ) fabricated with the LUMERA and LPKF laser systems, respectively. For both cases, the measured transmittance (markers) decreases linearly with the increase in LM filling fraction and is in strong agreement with the open-area model (dashed line; no data fitting). b) Transmittance spectra of the 4.5 μm LM grating patterns for various EGaIn filling fractions over the complete visible wavelength range. c) Optomechanical response of the patterned EGaIn conductor with a baseline transmittance of 85.3% (grating: $w = 4.5$ μm, $p = 96$ μm) under longitudinal and transverse strain showing the 550 nm wavelength transmittance versus strain. A slight (≈3.4%) increase in the transmittance of the LM conductor under the applied strain is directly related to the increase in transmittance of bare PDMS surface between the LM grid lines under tensile loading. Optomechanical response of bare PDMS substrate in which the biphasic metal coating has been fully ablated using the grating processing parameters is presented in the inset for comparison. d) Full spectral response of EGaIn film (grating: $w = 4.5$ μm, $p = 96$ μm) under various strain values. e) Optical images of visually imperceptible LM-conductor (grating: $w = 4.5$ μm, $p = 96$ μm) and clear PDMS film in the relaxed state and at 100% longitudinal strain.

and 50 μm wide traces as a function of varying LM filling fraction, which closely follow each other as well as fractional LM area (dashed line) calculated without the aid of data fitting.

Spectral dependence (wavelength: 380–860 nm) of the optical transmittance is plotted in Figure 3b for the case of the visually imperceptible LM-elastomer conductors (≈4.5 μm wide traces). These results show respectable optoelectronic responses—$T = 85.3\%$ at 2.95 Ω sq^{-1}, $T = 81.7\%$ at 1.71 Ω sq^{-1}, $T = 74.3\%$ at 0.84 Ω sq^{-1} and $T = 65.6\%$ at 0.55 Ω sq^{-1}—for an increasing filling fraction of liquid metal from 4.5% to 26.6%. The nearly flat spectra show that direct laser writing does not introduce specific wavelength losses across the visible band. The data show the electrical conductivity and optical transmittance to both rise monotonically as expected with the LM filling fraction. Thus, the filling area fraction model can be used to design the pattern geometry for desired optoelectronic performance suited to different applications.

Figure 3c presents the optomechanical response of the LM conductor selected with the highest initial transmittance (LM grating: $w = 4.5$ μm, $p = 96$ μm; T = 85.3%), presenting the transmittance at the most perceptible wavelength, $\lambda = 550$ nm, as a function of applied strain in the longitudinal and transverse directions. A small increase in the transmittance (3.4%) from 85.3% to 88.8% is observed with the increase in both types of applied strain. This is likely related to the optomechanical response of the bare PDMS surface between the LM grid lines, which was measured for samples in which the biphasic metal coating was fully ablated using the same laser processing parameters (Figure 3c inset and see discussion in Section S5, Supporting Information). Transmission response over the full visible wavelength at various peak strains is shown in Figure 3d and indicates that there is no significant optomechanical coupling with either longitudinal or transverse stretching. The left images in Figure 3e show a LM sample with an "invisible" (i.e., visually imperceptible) parallel-line grating with an optical transmittance of $T = 85.3\%$ and 88.7% in the relaxed ($\varepsilon = 0\%$) and stretched states ($\varepsilon = 100\%$), respectively. For comparison, optical images of a pristine PDMS substrate (no laser processing) are shown on the right with nearly 100% transmittance under the same conditions.

Lastly, we use AFM to measure the thickness, t, of the biphasic LM–Cu–Cr traces. This enables an estimate the effective volumetric resistivity ρ based on the measured sheet resistance $R_s = \rho/t$ of the conductive film. Based on the scan presented in Figure S9 of Section S6 (Supporting Information), the total film thickness is 600 nm (120 nm for the Cu–Cr layer and 480 nm for the LM coating). This implies that the $T = 85.3\%$ sample, which has a sheet resistance of 2.95 Ω sq^{-1}, has a resistivity of 1.77×10^{-6} Ω m. This low effective resistivity provides further evidence that the thermal ablative laser process does not degrade the intrinsic electrical properties of EGaIn or the biphasic metal architecture.

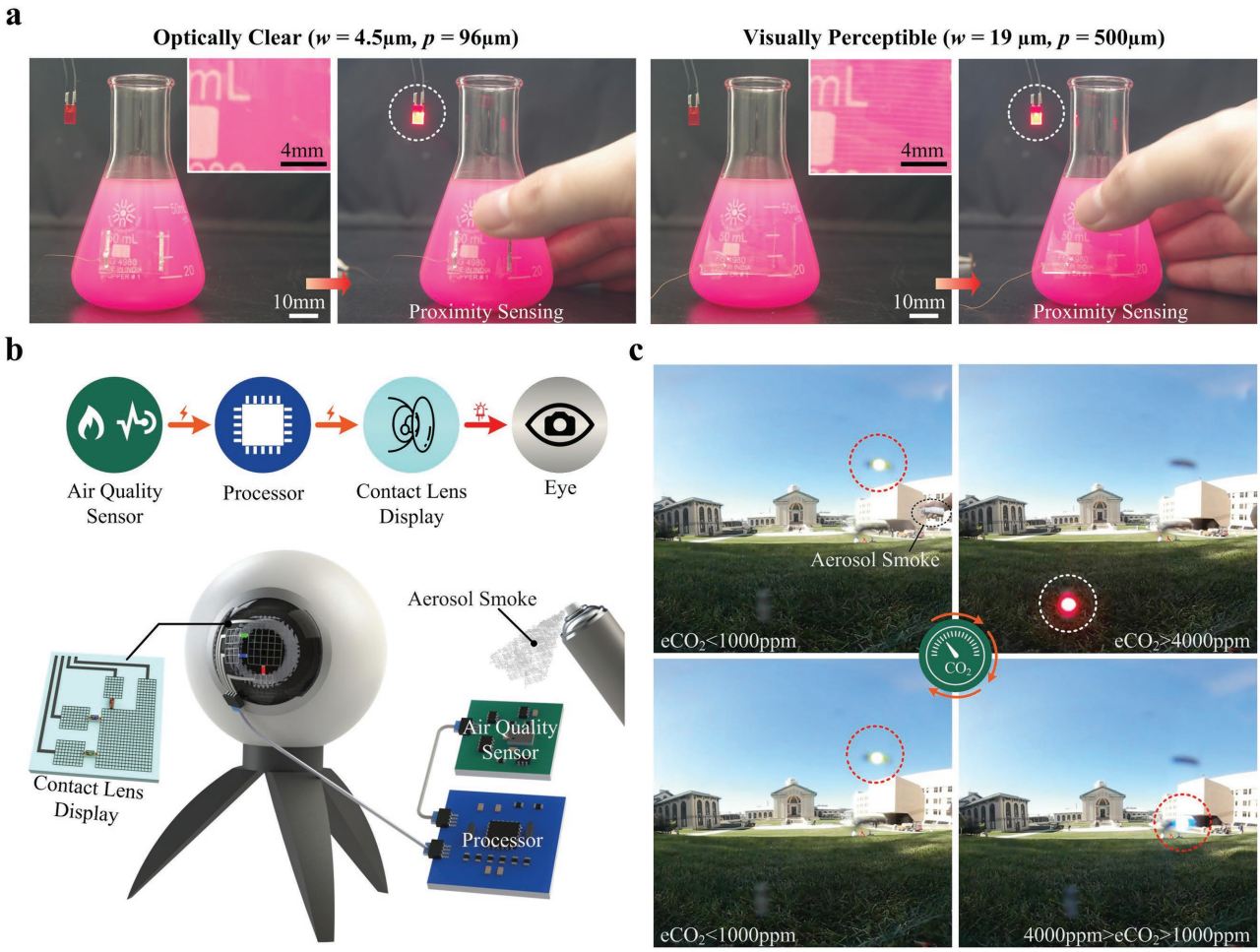

Figure 4. a) Proximity sensor using optically clear (w = 4.5 μm, p = 96 μm) and visually perceptible (w = 19 μm, p = 500 μm) conductor lines. b) Block diagram and schematic of air quality monitoring system composed of a contact lens display based on an LM circuit, an eyeball camera, an air quality sensor, and a microprocessor. c) Response sequence of air quality (CO_2) measurement corresponding to "SAFE"-green, "DANGEROUS"-red, "ALEART"-blue and "SAFE"-green. LED coloring is set according to eCO_2 thresholds set at <1000 ppm for "SAFE" and >4000 ppm for "DANGEROUS."

To demonstrate the potential of the present devices as soft transparent circuits in emerging "electronic skin" applications, several representative cases are illustrated. The first is an optically clear proximity sensor that can be placed on surfaces without causing visual interference. The transparent conductive film serves as a capacitive electrode for proximity sensing of a hand, triggering a capacitive touch sensor (CAP1188, Microchip) to light up an LED (see Experimental Section for details). The purpose here is to demonstrate electronic functionality on a curved surface while comparing the optical quality of circuits having 4.5 and 20 μm wide traces (pitch = 96, 500 μm, respectively). Both sensors are conformably bonded onto the curved surface of a flask using the inherent tackiness of the PDMS substrate. As demonstrated in **Figure 4**a, both proximity sensors detect the proximity of the hand to light the LED with equal success rates, indicating no difference in the functionality of each LM conductor (Movie S1, Supporting Information). However, the fully imperceptible LM sensor (4.5 μm wide wires) enables visual inspection of the hazardous material without obstruction.

The electrical functionality and compatibility with a curved surface is also demonstrated with a "smart contact lens" that can be used to display local air quality (Figure 4b,c). The circuit was mounted on a spherical camera to mimic a biological contact lens on the human eye. The circuit is visually imperceptible with 20 μm wide traces because the surface of the camera is outside of its focal plane—illustrating the importance of application context when selecting appropriate trace dimensions (see discussion in Section S1, Supporting Information). To demonstrate the air monitoring functionality of the circuit, the smart lens is sprayed with aerosol smoke containing carbon dioxide (CO_2) to mimic hazardous air quality. The air quality sensor (CCS811; AMS) detects the CO_2 concentration and reports an "equivalent calculated" carbon dioxide measure (eCO_2) to the microprocessor (ATmega328; Microchip). The microprocessor then illuminates an LED in the contact lens, corresponding to a designated air quality status. As shown in Figure 4c, before spraying, eCO_2 is less than 1000 ppm (threshold), corresponding to a green LED with an air quality status of "SAFE." After spraying, the eCO_2 count increases dramatically (>4000 ppm) and triggers the red LED to light up as a "DANGEROUS" indicator. With the diffusion of CO_2 to the environment, eCO_2 decreases and the signal switches from red to blue ("ALERT")

and finally back to green. The camera is able to record images through the LM circuit wiring without visual interference (only the embedded LED chips can be seen) due to its high optical transparency (Figure 4c; Movie S2, Supporting Information).

Transparent conductors with high elastic deformability and transparency typically suffer from significant electromechanical coupling and/or hysteresis. Here, we report a material architecture that overcomes this constraint and exhibits a unique combination of optoelectromechanical properties and is also well below the threshold for visual perception. The exceptional set of properties was accomplished with a laser micromachining process developed for high-resolution line patterning of liquid-phase EGaIn alloy on a soft and clear silicone elastomer. The low sheet resistance ($R_s = 2.95\ \Omega\ sq^{-1}$; resistivity = $1.77 \times 10^{-6}\ \Omega$ m), high transparency ($T > 85\%$ at 550 nm), high strain limit ($\varepsilon_{max} > 100\%$), and visual imperceptibility demonstrated here have never been observed before in other material systems. Moreover, the experimental results of transmittance were found to agree with predictions based on the geometry of traces without the aid of data fitting. Such simple modeling offers flexible tailoring of pattern design for desired optoelectronic responses. In addition, the results of cyclic tests demonstrated the mechanical robustness of transparent LM-elastomer systems. The combination of properties demonstrated here are attractive for enabling new applications in "second skin" wearable computing, human-computer interaction, and soft robotics that depend on soft, elastic, and optically transparent functionality.

Possible areas for improvement include further increase in transmission and conductivity, which can be captured by a figure of merit defined as $Z = T^{10}/R_s$.[41] For the samples presented here, Z is as high as 0.07 Ω^{-1}, which is comparable to ITO films but short of the highest values reported.[42] The transmission of the laser patterned LM conductor could potentially be improved by custom designing the laser scan path and optimizing the overlap between the adjacent scans (see Figure S7 in Section S4, Supporting Information). Another area of possible improvement relates to the speed and efficiency of fabrication. Currently, the subtractive laser-based fabrication process requires only 600 nm of metal film thickness to form conductive grid lines, thus ensures limited material waste during the commercial processing of large area circuits (i.e., 0.06 g of waste per 4 in. × 4 in. LM conductor). Material efficiency could be further improved with a thinner LM film, although this would be at the sacrifice of reduced conductivity. The circuit writing speed, which is currently 5 cm s^{-1} for single pulse aperture writing, can be increased dramatically by scaling to higher repetition rate, using beam multiplexing, and adopting more powerful ultrafast lasers.

Experimental Section

Substrate Preparation: The substrates were prepared by first spin coating a layer of polyvinyl alcohol (PVA 5 wt%; Ward's Science) onto a glass slide surface at 4000 rpm for 10 s. The film was dried in an oven at 70 °C for 30 s and then spin coated with PDMS (Sylgard 184, 10:1 ratio of base to curing agent; Dow Corning Corporation) at 600 rpm for 30 s. The thin layer of PVA was later used to release the final product, i.e., PDMS layer with patterned liquid metal (EGaIn, Ga 75%, In 25% by weight; Gallium Source LLC) from the glass slide. Next, the PDMS coating was vacuum cured at 70 °C for 1.5 h to obtain a 150 µm thick stretchable transparent substrate. To obtain a uniform thin layer of EGaIn, 20 nm thick chromium and then 100 nm thick copper layers were sputtered (Perkin Elmer 8L; PerkinElmer) onto the cured PDMS–glass substrates. The chromium coating served as the bonding layer between PDMS and copper. The copper coating formed an alloy with EGaIn when dipped in the liquid metal in the presence of sodium hydroxide solution (NaOH, 3 wt%) that was used to remove the oxide layers on copper and EGaIn to facilitate alloying. After 1 min of dip coating, the excess EGaIn was first removed under gravity by vertically pulling the substrate out of EGaIn/NaOH pool, followed by spinning the sample on a spin coater at 4000 rpm for 60 s. Finally, the sample was washed by DI water and isopropyl alcohol (99.5 wt%) for laser patterning. To fabricate LM grids without Cu–Cr underlayer, LM was directly roll-painted on PDMS substrate that resulted in ≈1 µm thick LM coating.

Laser Patterning: All samples with EGaIn line width greater than 10 µm were patterned by a 355 nm Nd:YAG laser (ProtoLaser U3; LPKF Laser & Electronics AG) using two ablation passes. The first pass with higher energy drove the most signification ablation to remove liquid EGaIn and solid metal (copper and chromium), whereas, the second pass with lower energy cleaned the dust and EGaIn ablation residue that was left behind on the PDMS surface after the first pass. For the first scan, the laser spot size of 15 µm was scanned with 0.5 W power (Power density, J = 0.28 MW cm^{-2}) at the repetition rate of 50 kHz, and mark speed of 150 mm s^{-1}, resulting in approximately 5 pulses per spot size. This laser ablation power was chosen such that the biphasic metal coating (LM–Cu–Cr) is completely removed with minimal damage to the exposed PDMS substrate (see Figure S10 in Section S6, Supporting Information, for LM patterning at different laser power densities). The same settings were applied for the cleaning step except with the power reduced to 0.25 W (0.14 MW cm^{-2}).

To reduce the line width below 10 µm, a solid-state Nd:YVO_4 ultrafast laser (Lumera, Hyper Rapid 50) was used to shrink the heat affected zone and improve the pattern resolution. The 1064 nm fundamental laser output with 12 ps pulse duration and 500 kHz repetition rate was focused onto the sample by a plano-convex lens of 25 mm focal length to an 8 µm focus spot size (M^2: 1.22) and Gaussian beam shape. The lens and sample were mounted to a linear XYZ motion stage (Aerotech, ABL10150/ABL10100/ALS130) for programmable scanning that could be synchronized with an electronic laser shutter to selectively turn on laser exposure at the sample area that required metal removal. After testing several exposure conditions, a first scan for laser ablation was applied with scanning speed of 50 mm s^{-1} and the laser frequency down-counted to 50 kHz of 5-pulse burst trains, which results in five pulses arriving at 500 kHz rate. The pattern ablation was followed with a second cleaning pass that was applied with the same exposure parameters except for the laser pulse energy reduced from 0.7 µJ (0.3 MW cm^{-2}) for the first ablation scan to 0.5 µJ (0.2 MW cm^{-2}) for the second cleaning scan.

Optomechanical Coupling Measurement: For optomechanical coupling measurement, laser patterned samples were encapsulated with PDMS to secure EGaIn traces. Uncured PDMS was poured to cover the substrate surface and then cured in wire-up position (gravity helps to remove the excess PDMS) at 70 °C for 1.5 h. Next, the sample was released from the glass substrate by scribing PDMS with a laser cutter (VLS3.50; Universal Laser System, Inc.) with the settings of 100% speed, 100% power, and 1000 ppi followed by mechanical peeling. The encapsulated samples were mounted on an acrylic holder and stretched to desired strains (0, 33.3%, 66.7%, 100%). After stretching to the desired strain, the samples were removed along with clamps and mounted into a UV–vis–NIR spectrometer (Perkin Elmer Lambda 900; PerkinElmer) to measure the transmittance across the 380–860 nm wavelengths. Clear PDMS film was used as the reference.

Electromechanical Coupling Measurement: To characterize electromechanical coupling in the laser-patterned samples, Velmex manual linear actuators were used to stretch samples to desired strains in the incremental steps of 5% strain (1 mm). The samples ends were

clamped to the actuators with textured 3D printed grips. Two EGaIn pads of LM pattern were covered by EGaIn pools, which were connected to copper probes for sheet resistance measurement by a micro-ohm meter (HP 34420A, Hewlett-Packard). The EGaIn traces were encapsulated with PDMS layer. The extremely thin layer of PDMS above the EGaIn pool was punctured to connect copper probes for measurements.

Surface Roughness and LM Grid Thickness: The vertical thickness (height) of patterned LM grid and surface roughness of the exposed PDMS surface after the laser ablation of metallic thin film was measured with NT-MDT atomic force microscope by Spectrum Instruments. The surface roughness measurements on LPKF and Lumera processed PDMS surface are carried out by the tapping-mode procedure, in which the driving frequency of the cantilever is adjusted around the resonance frequency of the cantilever (Nanoworld, NCHR-50). NT-MDT hybrid tapping mode is used to map the surface of the LM grid and measure the thickness of LM trace. In hybrid mode, the tip enters a force interaction with the sample thousands times per second. AFM height image and the cross-sectional view of patterned LM grid are presented in Figure S9 of Section S6 (Supporting Information). Topography maps of Lumera and LPKF processed PDMS surfaces are shown in Figure S6 of Section S4 (Supporting Information).

Proximity Sensor and Air Quality Monitoring: The imperceptible and transparent LM proximity sensors were wired to one of the channels of the capacitive touch sensor (CAP1188, Microchip). The corresponding channels LED driver was wired to an external LED to serve as a warning of possible danger to a human. An air quality sensor (CCS811, AMS) was used to determine the local air quality and warn the human of possible dangers. The sensor burn-in was performed for 48 h when first received and for 20 min before every test as described within the datasheet to ensure accurate readings. Based on the equivalent CO_2 output from the sensor a warning was displayed to the wearer by illuminating an LED mounted within the transparent display. The local air quality was modified using aerosol smoke (ESL Smoke! in a Can, Interlogix). The capacitive touch sensor and air quality sensor were interfaced with a microcontroller (ATmega328, Microchip) using the I^2C interface.

Supporting Information

Supporting Information is available from the Wiley Online Library or from the author.

Acknowledgements

C.F.P. and K.K. contributed equally to this work. This research was funded by the National Aeronautics and Space Agency (NASA ECF; Grant #: NNX14AO49G; Technical Contact: Dr. Bill Bluethmann). C.P. was supported by a grant from the Chinese Scholarship Council. The authors thank Kadri Bugra Ozutemiz for helpful discussions on the bi-phasic thin-film fabrication process.

Conflict of Interest

The authors declare no conflict of interest.

Keywords

direct laser writing, liquid-metal electronics, stretchable electronics, transparent conductors, visually imperceptible circuits

Received: November 27, 2017
Revised: December 27, 2017
Published online: February 6, 2018

[1] A. Abduev, A. Akmedov, A. Asvarov, A. Chiolerio, *Plasma Processes Polym.* **2015**, *12*, 725.
[2] M. S. Kim, C. H. Jeong, J. T. Lim, G. Y. Yeom, *Thin Solid Films* **2008**, *516*, 3590.
[3] J. Lewis, *Mater. Today* **2006**, *9*, 38.
[4] P. Görrn, M. Sander, J. Meyer, M. Kröger, E. Becker, H. H. Johannes, W. Kowalsky, T. Riedl, *Adv. Mater.* **2006**, *18*, 738.
[5] S. Savagatrup, E. Chan, S. M. Renteria-Garcia, A. D. Printz, A. V. Zaretski, T. F. O'Connor, D. Rodriquez, E. Valle, D. J. Lipomi, *Adv. Funct. Mater.* **2015**, *25*, 427.
[6] M. Stoppa, A. Chiolerio, *Sensors* **2014**, *14*, 11957.
[7] N. R. Armstrong, P. A. Veneman, E. Ratcliff, D. Placencia, M. Brumbach, *Acc. Chem. Res.* **2009**, *42*, 1748.
[8] Y. S. Park, K. H. Choi, H. K. Kim, *J. Phys. D: Appl. Phys.* **2009**, *42*, 235109.
[9] C. C. Kim, H. H. Lee, K. H. Oh, J. Y. Sun, *Science* **2016**, *353*, 682.
[10] C. Keplinger, J. Y. Sun, C. C. Foo, P. Rothemund, G. M. Whitesides, Z. Suo, *Science* **2013**, *341*, 984.
[11] J. J. Liang, L. Li, X. F. Niu, Z. B. Yu, Q. B. Pei, *Nat. Photonics* **2013**, *7*, 817.
[12] T. Sekitani, H. Nakajima, H. Maeda, T. Fukushima, T. Aida, K. Hata, T. Someya, *Nat. Mater.* **2009**, *8*, 494.
[13] A. Vásquez Quintero, R. Verplancke, H. De Smet, J. Vanfleteren, *Adv. Mater. Technol.* **2017**, *2*, 1700073.
[14] T. Stieglitz, W. Huang, S. C. Chen, J. W. Morley, N. H. Lovell, G. J. Suaning, presented at *2010 Annual Int. Conf. of the IEEE Engineering in Medicine and Biology*, Buenos Aires, August–September **2010**.
[15] D. J. Lipomi, M. Vosgueritchian, B. C. K. Tee, S. L. Hellstrom, J. A. Lee, C. H. Fox, Z. Bao, *Nat. Nanotechnol.* **2011**, *6*, 788.
[16] Z. B. Yu, X. F. Niu, Z. T. Liu, Q. B. Pei, *Adv. Mater.* **2011**, *23*, 3989.
[17] K. H. Kim, M. Vural, M. F. Islam, *Adv. Mater.* **2011**, *23*, 2865.
[18] K. S. Kim, Y. Zhao, H. Jang, S. Y. Lee, J. M. Kim, K. S. Kim, J.-H. Ahn, P. Kim, J. Y. Choi, B. H. Hong, *Nature* **2009**, *457*, 706.
[19] W. L. Hu, X. F. Niu, L. Li, S. Y. Yun, Z. B. Yu, Q. B. Pei, *Nanotechnology* **2012**, *23*, 344002.
[20] W. L. Hu, R. R. Wang, Y. F. Lu, Q. B. Pei, *J. Mater. Chem. C* **2014**, *2*, 1298.
[21] D. McCoul, W. L. Hu, M. M. Gao, V. Mehta, Q. B. Pei, *Adv. Electron. Mater.* **2016**, *2*, 1500407.
[22] H. Wu, L. Hu, M. W. Rowell, D. Kong, J. J. Cha, J. R. McDonough, J. Zhu, Y. Yang, M. D. McGehee, Y. Cui, *Nano Lett.* **2010**, *10*, 4242.
[23] H. Wu, D. Kong, Z. Ruan, P. C. Hsu, S. Wang, Z. Yu, T. J. Carney, L. Hu, S. Fan, Y. Cui, *Nat. Nanotechnol.* **2013**, *8*, 421.
[24] C. F. Guo, T. Sun, Q. Liu, Z. Suo, Z. Ren, *Nat. Commun.* **2014**, *5*, 3121.
[25] T. Gao, B. Wang, B. Ding, J. k. Lee, P. W. Leu, *Nano Lett.* **2014**, *14*, 2105.
[26] M. D. Dickey, *Adv. Mater.* **2017**, *29*, 1606425.
[27] M. Kubo, X. Li, C. Kim, M. Hashimoto, B. J. Wiley, D. Ham, G. M. Whitesides, *Adv. Mater.* **2010**, *22*, 2749.
[28] J. W. Boley, E. L. White, G. T. C. Chiu, R. K. Kramer, *Adv. Funct. Mater.* **2014**, *24*, 3501.
[29] A. Chiolerio, M. B. Quadrelli, *Adv. Sci.* **2017**, *4*, 1700036.
[30] Y. G. Moon, J. B. Koo, N. M. Park, J. Y. Oh, B. S. Na, S. S. Lee, S. D. Ahn, C. W. Park, *IEEE Trans. Electron Devices* **2017**, *64*, 5157.
[31] R. L. Levien, *Proc. SPIE* **2003**, *5293*, 405.
[32] C. A. Curcio, K. R. Sloan, R. E. Kalina, A. E. Hendrickson, *J. Comp. Neurol.* **1990**, *292*, 497.
[33] B. A. Gozen, A. Tabatabai, O. B. Ozdoganlar, C. Majidi, *Adv. Mater.* **2014**, *26*, 5211.

[34] I. D. Joshipura, H. R. Ayers, C. Majidi, M. D. Dickey, *J. Mater. Chem. C* **2015**, *3*, 3834.
[35] M. A. H. Khondoker, D. Sameoto, *Smart Mater. Struct.* **2016**, *25*, 093001.
[36] G. Li, X. Wu, D.-W. Lee, *Sens. Actuators, B* **2015**, *221*, 1114.
[37] H. J. Kim, T. Maleki, P. Wei, B. Ziaie, *J. Microelectromech. Syst.* **2009**, *18*, 138.
[38] A. Hirsch, H. O. Michaud, A. P. Gerratt, S. de Mulatier, S. P. Lacour, *Adv. Mater.* **2016**, *28*, 4507.
[39] T. Lu, E. J. Markvicka, Y. Jin, C. Majidi, *ACS Appl. Mater. Interfaces* **2017**, *9*, 22055.
[40] K. Sugioka, Y. Cheng, *Light: Sci. Appl.* **2014**, *3*, e149.
[41] G. Haacke, *J. Appl. Phys.* **1976**, *47*, 4086.
[42] Z. Chen, W. Li, R. Li, Y. Zhang, G. Xu, H. Cheng, *Langmuir* **2013**, *29*, 13836.